

Supporting information

A Porous Metal-Organic Framework with –COOH Groups for Highly Efficient Pollutant Removal

Qi Zhang, ^a Jiancan Yu, ^a Jianfeng Cai, ^a Ruijing Song, ^a Yuanjing Cui, ^a Yu Yang, ^a Banglin Chen^{*ab} and Guodong Qian^{*a}

^a State Key Laboratory of Silicon Materials, Cyrus Tang Center for Sensor Materials and Applications, Department of Materials Science & Engineering, Zhejiang University, Hangzhou 310027, China.

^b Department of Chemistry, University of Texas at San Antonio, San Antonio, TX 78249, USA.

Corresponding Authors:

Bangli.Chen@utsa.edu, gdqian@zju.edu.cn;

1.1 Materials and characterization.

All the chemicals were commercially available and used without further purification. ^1H NMR spectra were recorded on a Bruker Advance DMX 600 spectrometer using tetramethylsilane (TMS) as an internal standard. Thermogravimetric analyses (TGA) were carried out on a Netzsch TG209F3 with a heating rate of $1\text{ }^\circ\text{C}/\text{min}$ in N_2 atmosphere. Infrared spectrum (IR) was recorded on Thermo Fisher Nicolet iS10 spectrometer using KBr pallets. Raman spectra was recorded on BRUKER 81000 with a Ar^+ laser emitting at 532 nm in which a 2 mW output power was used in order to avoid sample decomposition. Elemental analyses for C, H, and N were performed on an EA1112 microelemental analyzer. Powder X-ray diffraction (PXRD) patterns were collected in the $2\theta = 5\text{--}50^\circ$ range on an X'Pert PRO diffractometer with $\text{Cu K}\alpha$ ($\lambda = 1.542\text{\AA}$) radiation at room temperature.

1.2 X-ray Crystallography

Single-crystal data were collected on Bruker Smart Apex II diffractometer with an Atlas detector using graphite-monochromatic $\text{Mo-K}\alpha$ radiation ($\lambda = 0.71073\text{ \AA}$) at 296 K. The determination of the unit cells and data collections for the crystal of **ZJU-24-0.89** were performed with CrysAlisPro. The data sets were corrected by empirical absorption correction using spherical harmonics, implemented in SCALE3 ABSPACK scaling algorithm. The structure was solved by direct methods, and refined by full-matrix least-square method with the SHELX-2013 program package. All non-hydrogen atoms including solvent molecules were located successfully from Fourier maps and were refined anisotropically. H atoms on C atoms were generated geometrically. The H atoms of the DMF molecules were clearly visible in different maps and were handled in the subsequent refinement with fixed isotropic displacement parameters. Crystallographic data are summarized in Table S1. CCDC XXXX contains the supplementary crystallographic data for this paper. These data can be obtained free of charge from The Cambridge Crystallographic Data Centre via www.ccdc.cam.ac.uk/data_request/cif.

1.3 Synthesis of ZJU-24 and NOTT-101

NOTT-101 was synthesized by a method as in ref.1

ZJU-24 compounds were obtained by adopting an otherwise identical procedure except for the different ratios of H_4TPTC and H_6TPHC . The synthesis of **ZJU-24-0.89** is thus presented here in detail as a representative: A mixture of H_4TPTC (1.86 mg), H_6TPHC (18.14 mg) and $\text{Cu}(\text{NO}_3)_2(\text{H}_2\text{O})_6$ (50.0 mg) was dissolved in DMF (6 mL) in a screw-capped vial. After stirring for 30 minutes, HCl (70 μL) and DI water (1 mL) were added to the mixture, the vial was capped and placed in an oven at $85\text{ }^\circ\text{C}$ for 72 h. The resulting blue crystals were collected by filtration and washed with DMF several times to give **ZJU-24-0.89**. Elemental analysis: Calcd. For $[\text{Cu}_2(\text{C}_{24}\text{H}_{12}\text{O}_{12})_{0.86}(\text{C}_{22}\text{H}_{10}\text{O}_8)_{0.14}(\text{H}_2\text{O})_2] \cdot 6\text{DMF} \cdot 2\text{H}_2\text{O}$ ($\text{Cu}_2\text{C}_{41.72}\text{H}_{61.72}\text{N}_6\text{O}_{21.44}$, %): C, 45.21; H, 5.34; N, 7.44; Found: C, 44.93; H, 5.59; N, 7.54.

The MOFs **ZJU-24** with other molar ratios of H_4TPTC and H_6TPHC (3:1, 1:1, 1:3, 1:20, and 0:1) were synthesized similarly to **ZJU-24-0.89** except for the use of a mixture of H_4TPTC and H_6TPHC .

1.4 Details of MB adsorption test

Before adsorption, **ZJU-24-0.89** and **NOTT-101** was dried overnight under vacuum at $100\text{ }^\circ\text{C}$ and kept in a desiccator. Then the adsorbent (5 mg) was weighed precisely. During the adsorption process, adsorbents (5 mg) were used for the removal of MB with the concentrations of 5 ppm. The dye solutions (50 mL) containing the adsorbents were mixed well with magnetic stirring and maintained for a fixed time (5 min to 12 h) at $25\text{ }^\circ\text{C}$. The solution was separated from the adsorbent with a syringe filter (PTFE, hydrophobic, $0.5\text{ }\mu\text{m}$) for calculation of dye concentration by comparing the UV-vis absorbance (at $\lambda = 665\text{ nm}$) to the calibration curve. Effect of H_6TPHC content in the **ZJU-24** series for the removal of MB was tested with the same method.

To obtain the adsorption capacity, **ZJU-24-0.89** (5 mg) was dispersed in 50 mL of MB solutions with a known dye concentration between 20 and 250 ppm. 12 hours later, the solution was separated from the adsorbent with a syringe filter and Ultraviolet spectroscopy was used to analyze the residual concentrations of MB. The equilibrium adsorption capacity Q_e was calculated according to Eq. (1):

$$Q_e = \frac{(C_0 - C_e)V}{m} \quad (1)$$

Where C_0 and C_e (mg/L) were the initial and final concentrations of MB, respectively. V (L) was the volume of the solution, and m (g) was the mass of sorbent.

1.5 Molecular Simulation Studies

Simulated calculations were performed with Material Studio 7, using the Forcite module. Configurations were explored for calculation (Figure S14). After geometry optimization, for **ZJU-24**, the total energy is determined to be 109.79 kcal / mol lower than **NOTT-101**, which testifies **ZJU-24** is more efficient for the absorption of MB molecules.

To work out the optimal configuration of MB molecule, structure of **ZJU-24** was immobilized except for the middle benzene ring and carboxyl groups on it. The outcome of geometry optimization reveals a 4.8 ° rotation of the middle benzene ring, $\text{C}=\text{O}$ changes from 1.076 \AA to 1.273 \AA , $\text{C}-\text{O}$ changes from 1.178 \AA to 1.293 \AA after interaction with MB molecule (Figure S15).

Table S1. Crystallographic Data collection and Refinement result for **ZJU-24-0.89**.

	ZJU-24-0.89
chemical formula	C ₂₄ H ₈ Cu ₂ O ₁₄
formula weight	647.38
temperature (K)	296(2)
wavelength (Å)	0.71073
crystal system	Trigonal
space group	R-3m
<i>a</i> (Å)	18.6935(7)
<i>b</i> (Å)	18.6935(7)
<i>c</i> (Å)	38.3901(12)
α (°)	90
β (°)	90
γ (°)	120
<i>V</i> (Å ³)	11618.0(9)
<i>Z</i>	9
density (calculated g/cm ⁻³)	0.833
absorbance coefficient (mm ⁻¹)	0.860
<i>F</i> (000)	2898
crystal size (mm ³)	0.30 × 0.26 × 0.20
goodness of fit on <i>F</i> ₂	1.079
R1, wR2 (<i>I</i> > 2σ(<i>I</i>)) ^a	0.0494, 0.1768
R1, wR2 (all data) ^a	0.0717, 0.1940
largest difference peak and hole (e/Å ³)	0.600, -0.354
^a R1 = Σ(<i>F</i> _o - <i>F</i> _c) / Σ <i>F</i> _o ; wR2 = [Σw(<i>F</i> _o - <i>F</i> _c) ² / Σw <i>F</i> _o ²] ^{1/2} .	

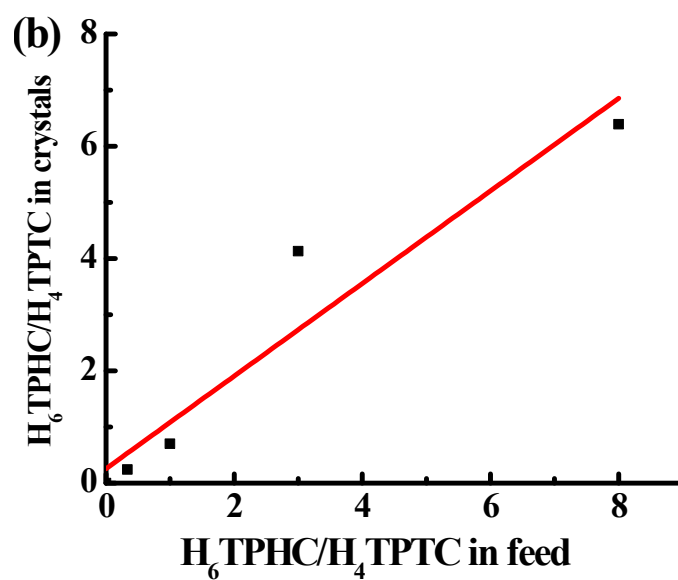
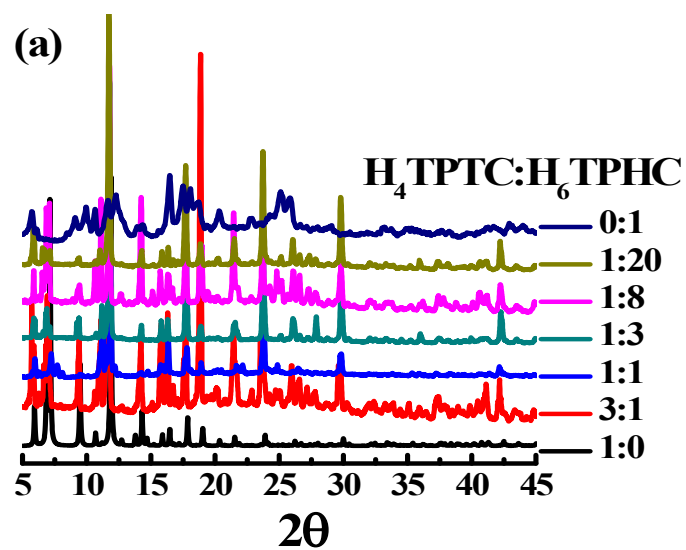


Figure S1. (a) PXRD data for **ZJU-24** prepared from various feed ratios of H_4TPTC and H_6TPHC (1:0, 3:1, 1:1, 1:3, 1:8, 1:20, and 0:1); (b) Plot of H_6TPHC/H_4TPTC in crystals vs H_6TPHC/H_4TPTC in feed.

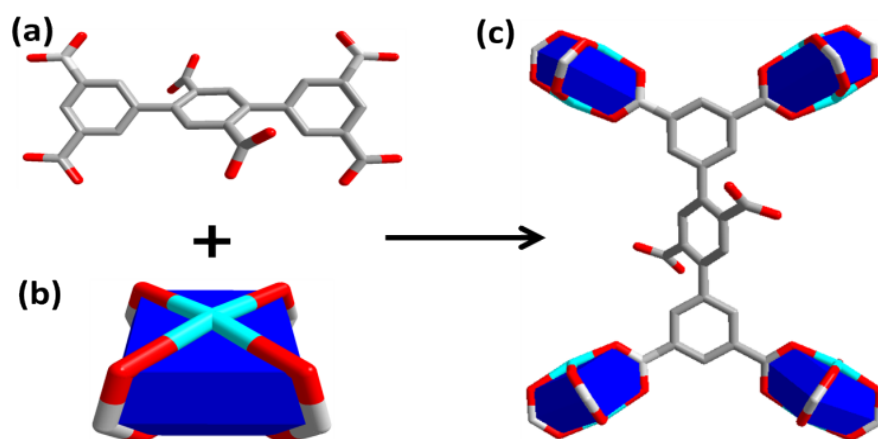


Figure S2. Illustration of the functionalization: (a) the ligand H₆TPHC and (b) paddle wheel SBU in **ZJU-24**; (c) each ligand coordinate four SBUs, (Cu: blue; C: grey; O: red).

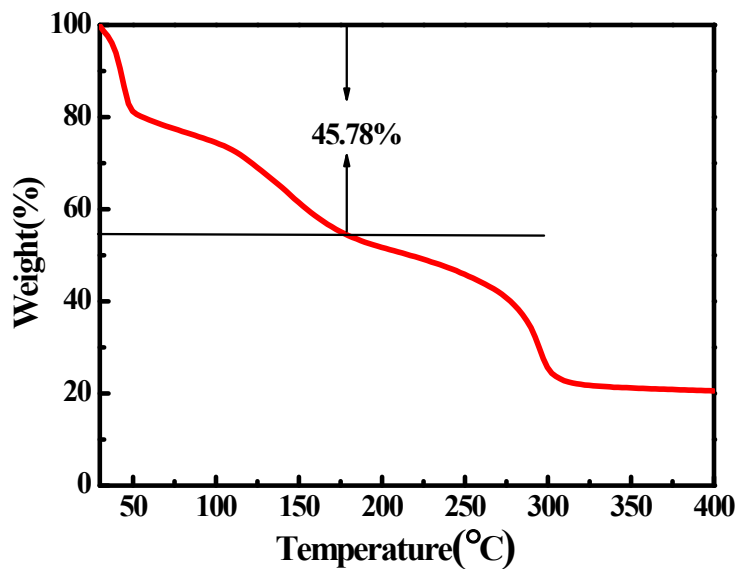
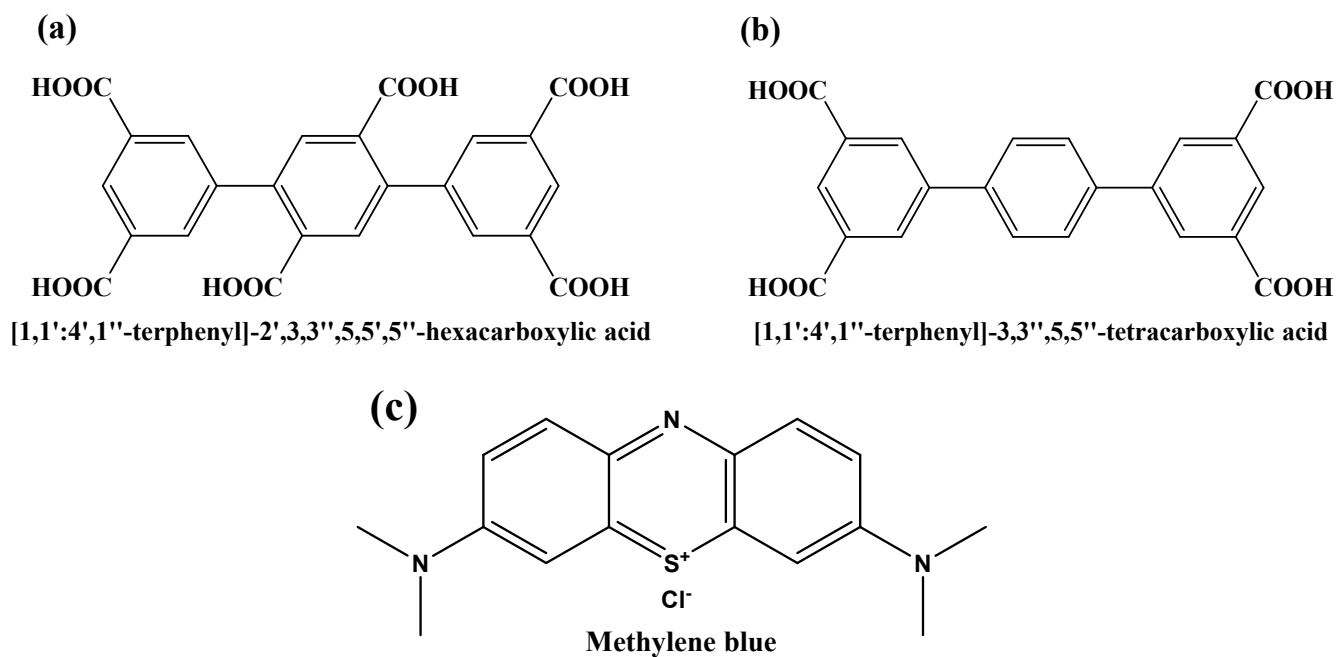


Figure S3. TGA curves of as-synthesized **ZJU-24-0.89** under a nitrogen atmosphere at a heating rate of 1 K min⁻¹.



Scheme s1 (a) H₆TPHC, (b) H₄TPTC and (c) MB

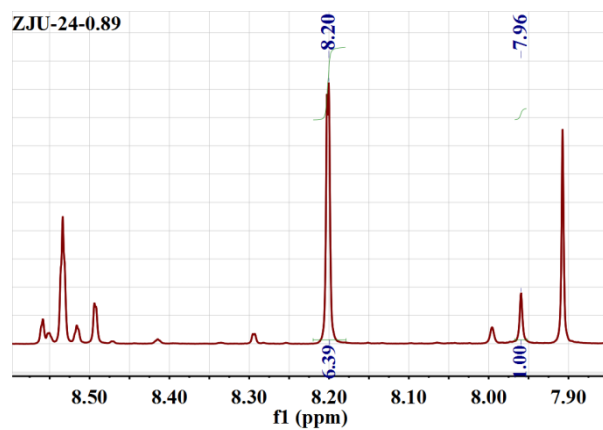
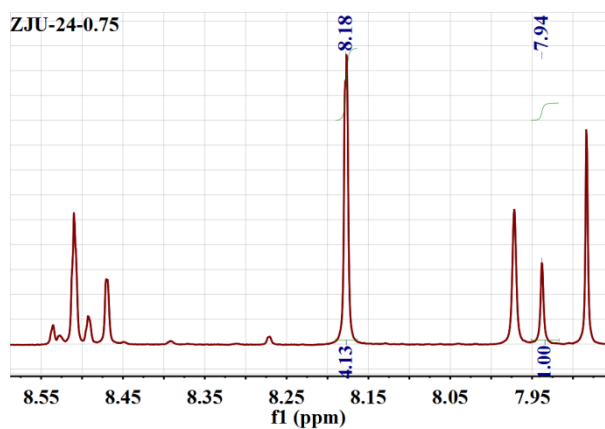
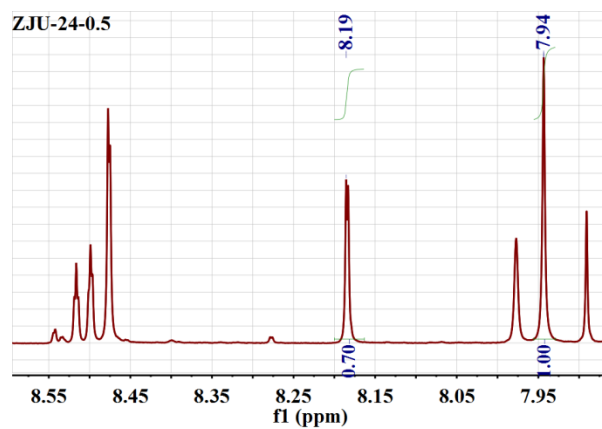
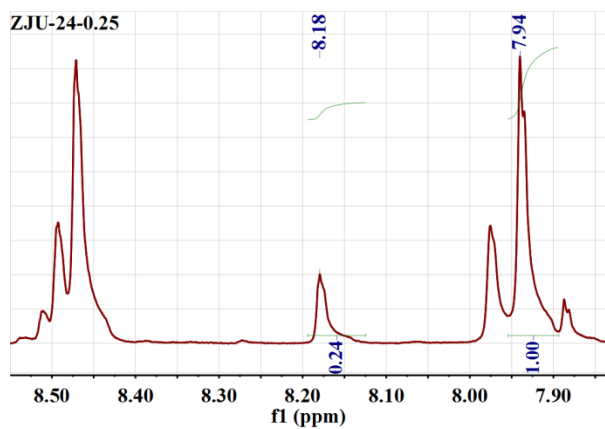


Figure S4. NMR analysis of ZJU-24-0.25, ZJU-24-0.5, ZJU-24-0.75, ZJU-24-0.89.

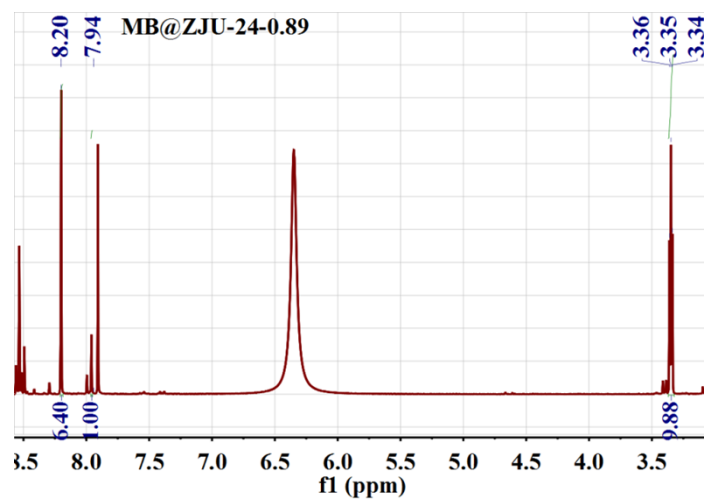


Figure S5. NMR analysis of MB and ligand ratio in ZJU-24-0.89 \supset MB crystals.

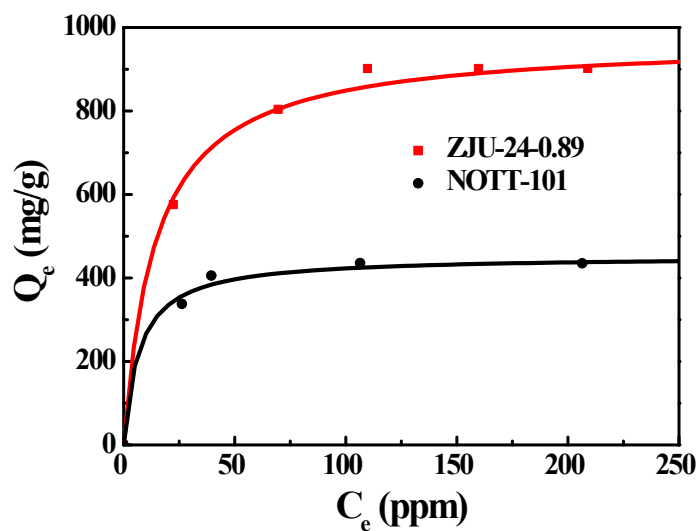


Figure S6. Adsorption isotherms for MB adsorption over **ZJU-24-0.89** and **NOTT-101**, C_e : equilibrium concentration of adsorbate, Q_e : the amount of adsorbate adsorbed.

Table S2. Adsorption capacities for MB on various porous materials.

Material	Absorption capacity for MB [mg/g]	T [K]	Ref.
ZJU-24	902	298	This work
Amino-MIL-101(Al)	762	303	2
Ordered mesoporous carbons	758	298	3
Co/NPC derived from ZIF-67	503	298	4
graphene oxide sponge	397	298	5
activated carbons	396	298	3
POM@MIL-101	371	298	6
MIL-101(Al)	195	303	2
MOF-235	187	298	7
MOF–graphite oxide composite	183	298	8
Superabsorbent hydrogel	48	298	9

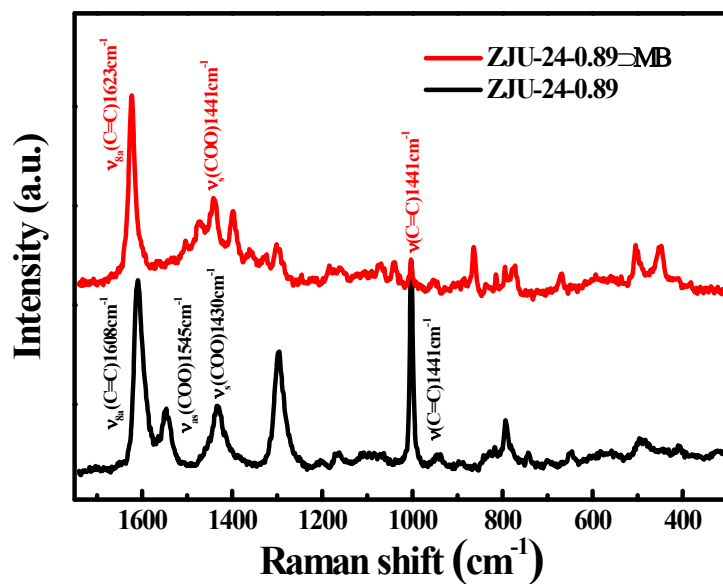


Figure S7. Raman spectra of the crystal before and after MB adsorption with a $\lambda=532$ nm laser.

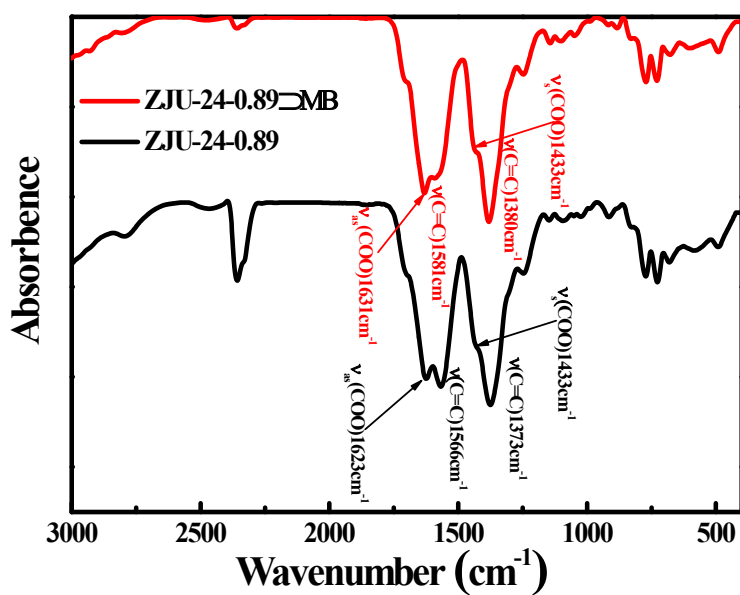


Figure S8. FT-IR spectra of the crystal before and after MB adsorption.

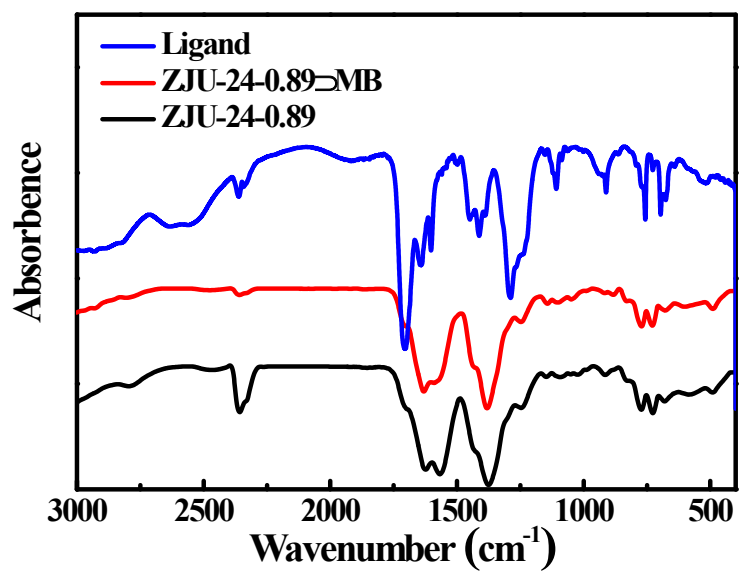


Figure S9. FT-IR spectra of ZJU-24-0.89, ZJU-24-0.89MB and ligand.

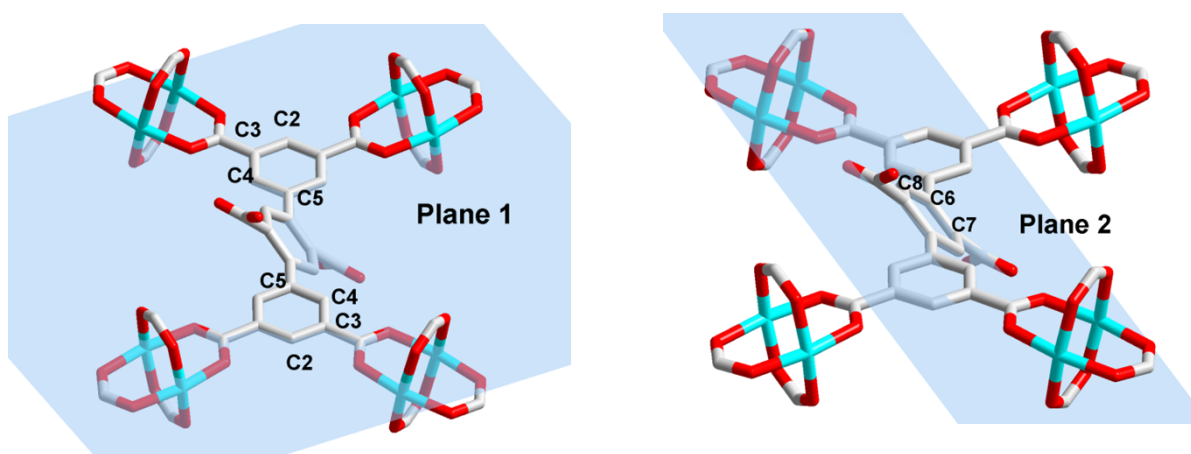


Figure S10. Illustration of plane 1 and 2.

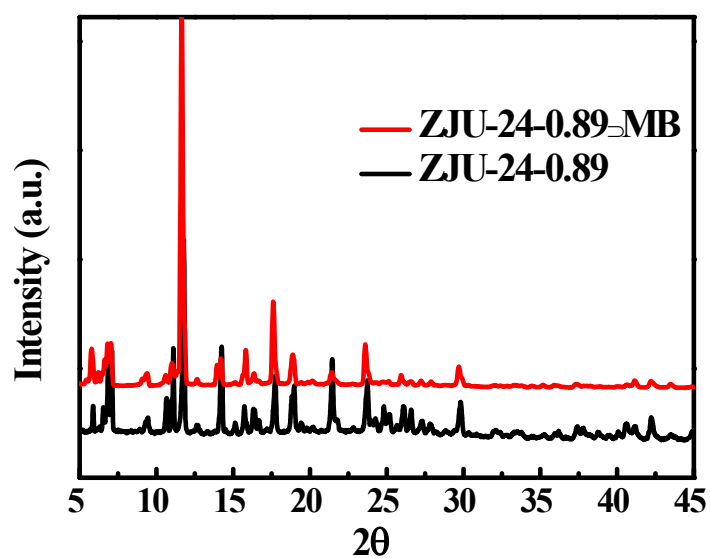


Figure S11. PXRD data for ZJU-24-0.89 and ZJU-24-0.89MB.

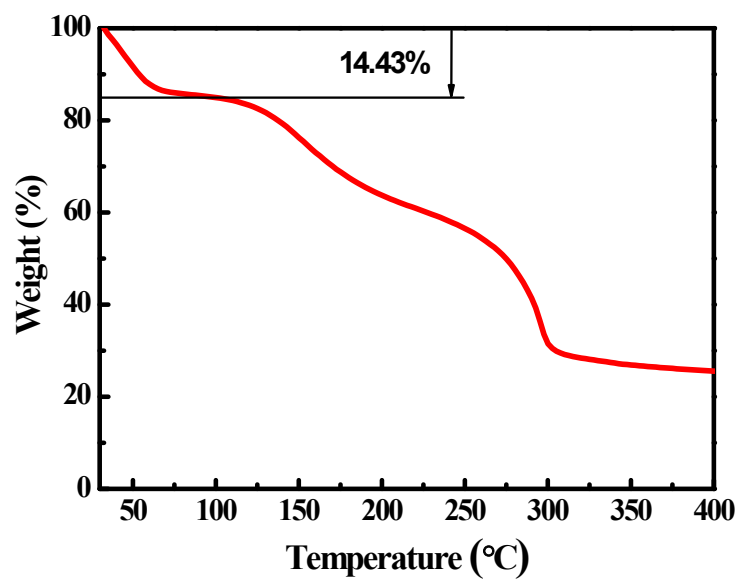


Figure S12. TGA curves of ZJU-24-0.89MB under a nitrogen atmosphere at a heating rate of 1 K min⁻¹.

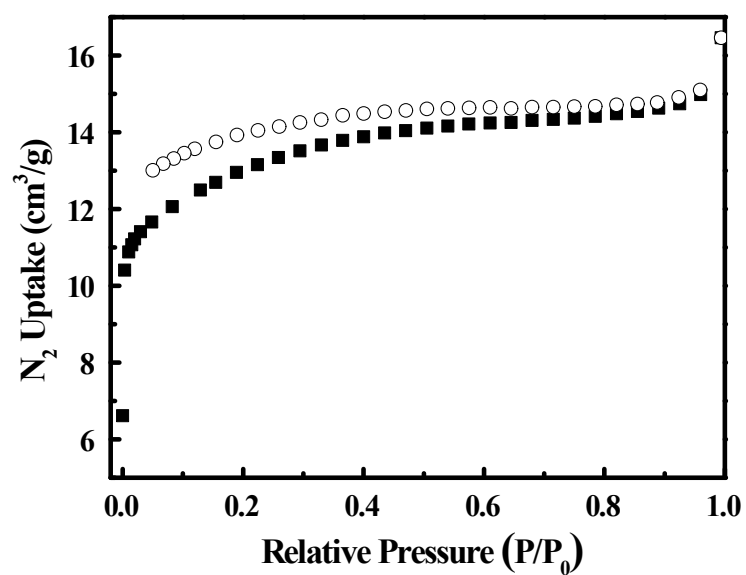


Figure S13. N_2 sorption isotherms of **ZJU-24-0.89MB** at 77 K (solid symbols: adsorption, open symbols: desorption).

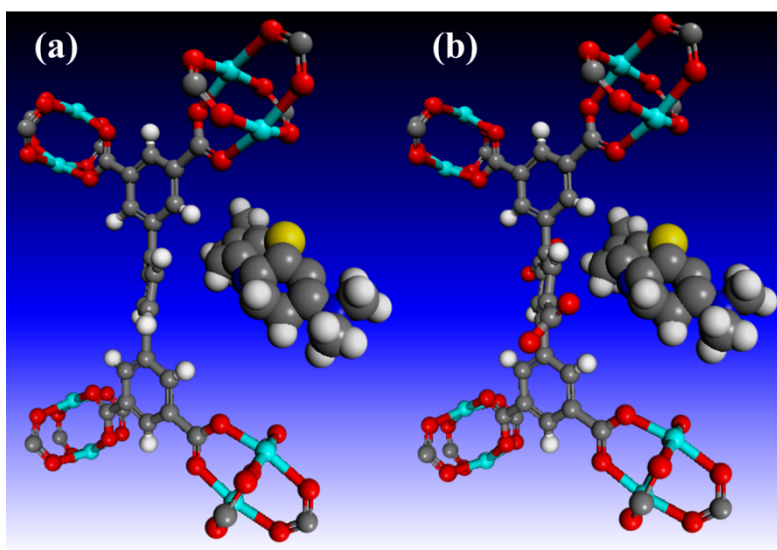


Figure S14. Illustration of configurations used for simulated calculation: (a) configuration for **NOTT-101**; (b) configuration for **ZJU-24**.

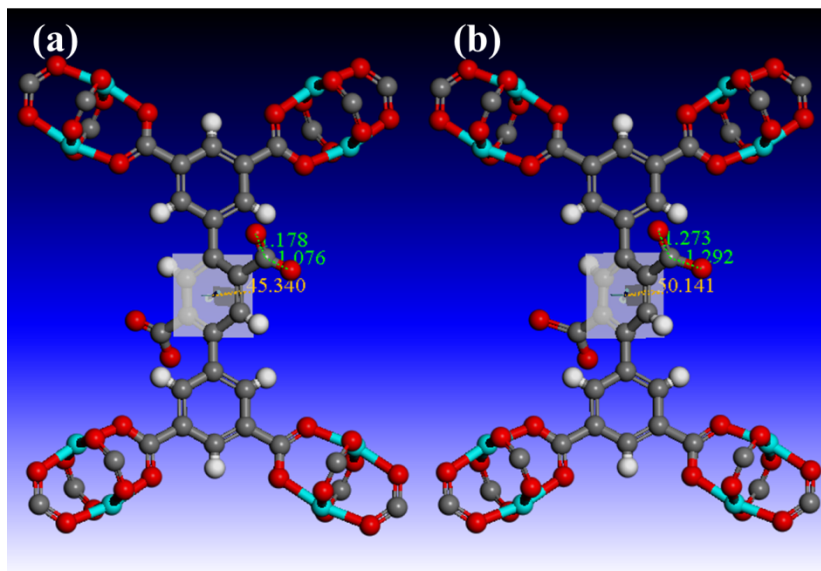


Figure S15. Structure changes of **ZJU-24** after geometry optimization: (a) geometry optimization without MB; (b) geometry optimization with the effect of MB.

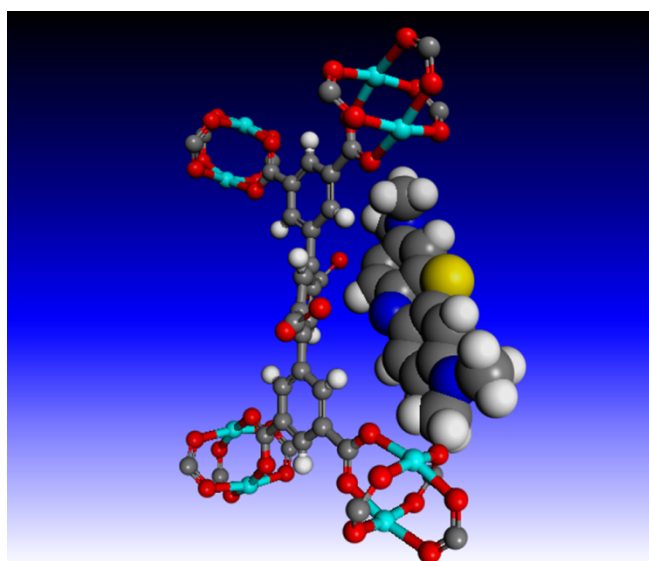


Figure S16. Outcome of geometry optimization with the presence of MB molecule.

REFERENCES

- 1 X. Lin, I. Telepeni, A. J. Blake, A. Dailly, C. M. Brown, J. M. Simmons, M. Zoppi, G. S. Walker, K. M. Thomas, T. J. Mays, P. Hubberstey, N. R. Champness and M. Schröder, *J. Am.Chem.Soc.*, 2009, **131**, 2159.
- 2 E. Haque, V. Lo, A. I. Minett, A. T. Harris and T. L. Church, *J. Mater. Chem. A*, 2014, **2**, 193.
- 3 X. Zhuang, Y. Wan, C. Feng, Y. Shen and D. Zhao, *Chem. Mater.*, 2009, **21**, 706.
- 4 N. L. Torad, M. Hu, S. Ishihara, H. Sukegawa, A. A. Belik, M. Imura, K. Ariga, Y. Sakka and Y. Yamauchi, *Small*, 2014, **10**, 2096.
- 5 F. Liu, S. Chung, G. Oh and T. S. Seo, *ACS Appl. Mater. Interfaces.*, 2011, **4**, 922.
- 6 A.-X. Yan, S. Yao, Y.-G. Li, Z.-M. Zhang, Y. Lu, W.-L. Chen and E.-B. Wang, *Chem. Eur. J.*, 2014, **20**, 6927.
- 7 E. Haque, J. W. Jun and S. H. Jhung, *J. Hazard. Mater.*, 2011, **185**, 507.
- 8 L. Li, X. L. Liu, H. Y. Geng, B. Hu, G. W. Song and Z. S. Xu, *J. Mater. Chem. A*, 2013, **1**, 10292.
- 9 A. T. Paulino, M. R. Guilherme, A. V. Reis, G. M. Campese, E. C. Muniz and J. Nozaki, *J. Colloid Interface Sci.*, 2006, **301**, 55.